Revisiting Acido-basicity of the MgO Surface by Periodic Density Functional Theory Calculations: Role of Surface Topology and Ion Coordination on Water Dissociation

Céline Chizallet,*,† Guylène Costentin,† Michel Che,†,§ Françoise Delbecq,‡ and Philippe Sautet*,‡

Laboratoire de Réactivité de Surface, UMR 7609 CNRS, Université Pierre et Marie Curie, 4 place Jussieu, 75252 Paris Cedex 05, France, Laboratoire de Chimie, UMR 5182 CNRS, Ecole Normale Supérieure de Lyon, 46 allée d'Italie, 69364 Lyon Cedex 07, France, and Institut Universitaire de France, 103 bd Saint-Michel 75005, Paris, France

Received: February 9, 2006; In Final Form: June 8, 2006

Low-coordinated (LC) ions at the MgO surface (noted Mg^{2+}_{LC} and O^{2-}_{LC} with L = 1−5), located on monatomic and diatomic steps, corners, step divacancies, and kinks, have been modeled thanks to periodic density functional theory (DFT) calculations (VASP). Ions of lowest coordination induce the strongest surface geometry relaxation and the highest surface energies. The hydration energies of these sites and thermodynamic stabilities of the resulting surfaces were studied. The factors controlling the interaction strength between water and the surface are the possibility for the hydroxyl group to adopt a bridging geometry between two Mg^{2+} cations in concave areas of the surface, such as the bottom of the monatomic step, and at second order the surface atomic coordination, and especially the presence of three-coordinated ions. The Lewis basicity and acidity of O^{2-}_{LC} and Mg^{2+}_{LC}, respectively, increase as their coordination number decreases, which implies the same trend for the Brønsted basicity of the $Mg^{2+}-O^{2-}$ pair toward water. However, this trend can be changed if pairs leading to the formation of bridging OH groups are involved, typically on monatomic steps or in step divacancies where $O_{2C}-H$ and $O_{3C}-H$ are obtained, respectively, instead of the expected $O_{1C}-H$. Thanks to thermodynamic calculations, the state of the surface as a function of temperature can be determined at a given pressure, unraveling the roles of surface topology and ions coordination.

1. Introduction

Numerous experimental and theoretical studies in the fields of surface science and catalysis are devoted to the description of the reactivity of MgO. Despite its simple rocksalt structure, its surface geometry and behavior toward various atmospheres are far from obvious. In particular, the study of powdered samples is complex due to various crystallographic planes likely to appear. Nevertheless, the important interest for highly divided samples as catalysts[1−3] requires information on the various sites likely to react on their surface. Moreover, MgO exposed to water exhibits high reactivity in several basic-catalyzed reactions:[1,4−8] the nature of the species generated upon water adsorption on divided MgO samples has thus to be examined to identify the most active species for a given catalytic process.

The (100) plane exhibits the higher thermodynamic stability,[9] but due to the variety of conditions used for the oxide synthesis, less stable structures appear on the surface. Che and Tench[10] proposed a model for the real MgO surface, exhibiting low-coordinated (LC) ions, referred to as O^{2-}_{LC} or Mg^{2+}_{LC}. Their coordination number depends on their location on the surface (L = 3, corners; L = 4, edges; L = 5, terraces). From extensive theoretical study of water adsorption on the (100) surface, it is well established that terraces do not dissociate an isolated water molecule,[11−13] whereas one-third of the molecules dissociate in the monolayer,[11,12,14−17] which is confirmed experimentally.[18,19] Defect rich surfaces interact more strongly with water, as shown by TPD[20,21] and UPS.[22,23] Adsorption energies of water on edges (exhibiting 4C ions) are always higher than on (100) planes and correspond to water dissociation.[24−29] This trend is even increased with 3C ions.[24,27] However, a systematic ab initio study of defects involving 4C and 3C ions described in a realistic way, of their interaction with water, of the geometry and thermal stability of the resulting hydroxyls, is lacking. The hydroxyls generated by dissociation of water on $Mg^{2+}_{LC}-O^{2-}_{L'C}$ pairs are expected to be formed according to eq 1:

$$Mg^{2+}_{LC}\text{-}O^{2-}_{L'C} + H_2O \rightleftharpoons \overset{OH^-}{\underset{|}{}}\ \overset{H^+}{\underset{|}{}}\ Mg^{2+}_{LC}\text{-}O^{2-}_{L'C} \quad (1)$$

Two main categories of hydroxyls are expected: $O_{L'C}H$ groups generated by protonation of surface oxide anions and OH groups issued from the hydroxylation of surface magnesium cations Mg^{2+}_{LC}, usually referred to as multicoordinated and monocoordinated OH groups, respectively. Their properties are expected to depend not only on L and L′ but also on the amount of hydrogen bonding between them. One may wonder if the hydroxyls classification proposed by Knozinger[30] on the basis of IR characterization exhaustively describes the geometry of all OH groups existing on an irregular MgO surface.

Moreover, the affinity of surface defects toward a protic molecule like water raises the question of their Brønsted basicity. Deprotonation of water involves the Brønsted basicity of $O^{2-}_{L'C}$, and the neighboring Mg^{2+}_{LC}, behaving as a Lewis acid, stabilizes the HO^- moiety. Are coordination numbers accurate parameters

* To whom correspondence should be addressed. Tel.: +33 1 44 27 60 05. Fax: +33 1 44 27 60 33. E-mail: chizalle@ccr.jussieu.fr (C.C.); Philippe.Sautet@ens-lyon.fr (P.S.).

† Université Pierre et Marie Curie.

‡ Ecole Normale Supérieure de Lyon.

§ Institut Universitaire de France.

10.1021/jp060840l CCC: $33.50
Published on Web 07/20/2006

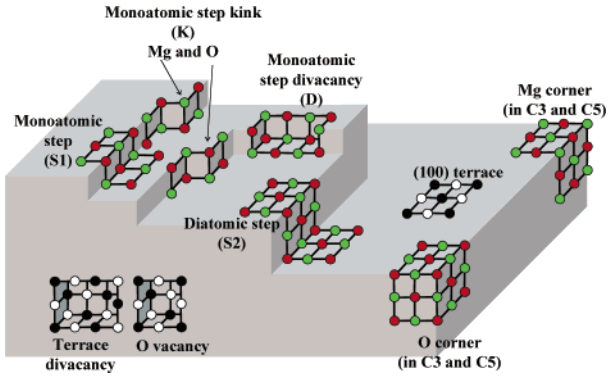

Figure 1. Schematic representation of the irregularities on the MgO surface. The steps and corners model, proposed earlier by Che and Tench,[10] is adapted here to the systems discussed. Defects modeled in the present work are shown with red (O^{2-}) and green (Mg^{2+}) spheres, whereas the systems in black (O^{2-}) and white (Mg^{2+}) will not be the object of further calculations here (see text). The terminology used for the modeled systems is reported in brackets; see section 2.2.1 and Figure 2: S1 depicts the monatomic step, S2 the diatomic step, C3 and C5 the corner system (depending on the length between $Mg^{2+}{}_{3C}$ and $O^{2-}{}_{3C}$), D the monatomic step divacancy, and K the kinks.

to classify the deprotonating ability of the $Mg^{2+}{}_{LC}-O^{2-}{}_{L'C}$ pair? Experimental work performed on methanol shows that the Brønsted basicity of the surface increases with its irregularity.[1] This observation made at the macroscopic level needs to be substantiated at the molecular level.

DFT calculations have shown to be a powerful tool to describe the thermal stability of hydrated oxide surfaces.[31,32] Because terraces,[11,12,14−17] oxygen vacancies,[13,33] and terrace divacancies,[34] shown in black (O^{2-}) and white (Mg^{2+}) in Figure 1, have already been extensively studied, no further calculations are performed on these systems in the present work, which focuses on the study of MgO surface irregularities. The systems studied, chosen in relation to experimental observations, are schematized in red (O^{2-}) and green (Mg^{2+}) in Figure 1. Monatomic and higher steps have been evidenced on model MgO surfaces by AFM[22,23,35−38] and X-ray studies.[39,40] Higher steps differ from monatomic steps by the distinct behavior of their edges and the valley at their bottom. Monatomic and diatomic steps (considered as representative of higher steps on the basis of preliminary work[41]) will be studied here for the sake of comparison with other defects. The edges of diatomic steps are also model edges of cubic particles, obtained by oxidation of metallic magnesium.[42−44] Their corners can be terminated by either $O^{2-}{}_{3C}$ or $Mg^{2+}{}_{3C}$ ions, at the meeting points of three extended edges. These edges can sometimes be smaller, providing more confined systems containing 3C ions and corresponding to kinks (with either $O^{2-}{}_{3C}$ or $Mg^{2+}{}_{3C}$ terminations) or divacancies in monatomic steps that are expected to be representative of a high concentration of 3C ions observed on MgO obtained by sol−gel routes, for example.[44] The (110) and (111) surfaces are not considered as they seem to reconstruct to form steps[45,46] and (100) microfacets terminated by 3C ions, in similar local environment than corners,[47−49] respectively.

The aim of the present work is thus to study the structure of surface defects and their behavior toward water by quantum chemical calculations, in the framework of the DFT for periodic systems. The strength of the interaction with water is also discussed in terms of relative Brønsted basicity of the surface defects and individual ions. The stability of the OH groups formed is studied and the state of the hydrated surface described as a function of preparation conditions, such as temperature and pressure.

2. Computational Methods

2.1. Methods. The calculations are performed in the framework of the DFT and the generalized gradient approximation exchange-correlation functional of Perdew and Wang PW91,[50] as implemented in the Vienna Ab Initio Simulation Package (VASP 4.6).[51,52] The one electron wave function is developed on a basis set of plane waves, and the interaction between the core and the valence electrons is described by the projector augmented waves (PAW) approach.[53] The selected description of the oxygen atomic core allows a good convergence on the energy for a cutoff of 265 eV (increasing cutoff at 400 eV induces hydration energy variations lower than 3%). The convergence criterion for the electronic self-consistent cycle is fixed to 10^{-6} eV per supercell. Geometry optimizations are performed within a conjugate-gradient algorithm until the convergence criterion on forces (10^{-2} eV·Å^{-1}) is reached. A net dipole leading to a spurious electrostatic interaction between the slab and its periodic images along the *z* axis (see below) may be induced. A dipolar correction along the perpendicular to the slab is applied to remove this effect. This correction does not exceed 0.05‰ of the total cohesive energy.

2.2. Surfaces. *2.2.1. Systems Containing 4C and 3C Ions.* Irregularities on MgO surfaces are modeled by a slab approach using periodic boundary conditions. Their characteristics without any relaxation (bulk-terminated geometry), the terminology used (also denoted on Figure 1), and the axes orientations are reported in Table 1 and shown in Figure 2.

4C ions are described by monatomic steps (terraces size, three times d_{Mg-O}, the Mg−O bond length in the lattice, Figure 2a), referred to as S1, and diatomic steps (terraces size, $2d_{Mg-O}$, Figure 2b), are called S2. The S1 and S2 slabs are composed of three layers of ions, which was proved to provide a converged description of the electronic structure for MgO(100).[54] 3C ions are modeled by the corner systems C3 and C5, with the respective length of the edge between $O^{2-}{}_{3C}$ and $Mg^{2+}{}_{3C}$ (Figure 2c) of $3d_{Mg-O}$ and $5d_{Mg-O}$. These systems allow for the simultaneous simulation of $O^{2-}{}_{3C}$ and $Mg^{2+}{}_{3C}$-terminated corners. 3C ions in a more confined environment are modeled by a divacancy, referred to as D (first studied by Pisani and co-workers[55]), performed on the edge of S1 (Figure 2d), and by kinks, called K, also performed on S1 by formally removing four atoms in its edge. The value of d_{edge} (Figure 2d) is the main difference between D ($d_{edge} = 3d_{Mg-O}$) and K ($d_{edge} = 5d_{Mg-O}$). K models simultaneously $O^{2-}{}_{3C}$ and $Mg^{2+}{}_{3C}$-terminated kinks. For S1, S2, D, and K, the lowest layer of ions is constrained at the bulk geometry, whereas the other ones are allowed to relax. For the bigger C3 and C5 models, the first and second neighbors of surface ions on the edge between $O^{2-}{}_{3C}$ and $Mg^{2+}{}_{3C}$ are relaxed.

2.2.2. Hydration. The edge of the steps is hydrated at various coverage, without any hydration of the terraces, as observed experimentally at low water pressure.[16,18] One or two molecules are adsorbed on C3 and C5. D and K are monohydrated. The oxygen and hydrogen atoms coming from water are relaxed, in addition to the ions relaxed in dehydrated systems. Hydrated systems are named as follows: system−n_{ads}w, where n_{ads} stands for the number of water molecule per unit cell. Two configurations of S1−1w are studied: S1−1w−H and S1−1w-*n*H correspond to nearby and distant hydroxyls, respectively (see Figure 3). For S2, the hydration on the edge or in the valley leads to S2−ON−n_{ads}w (ON means on the edge) and S2−IN−n_{ads}w (IN means in the valley), respectively (see Figure 4). The adsorption of a single water molecule on C3 takes place on either $O^{2-}{}_{3C}$ or $Mg^{2+}{}_{3C}$, leading to C3−1w−O_{3C} and C3−1w−

TABLE 1: Systems, Terminology, and Parameters Used for the Simulation of MgO Surface Defects and the Resulting Surface Energy After Relaxation

	steps		corners		step vacancies	
system	monatomic	diatomic	4-atoms edge	6-atoms edge	divacancy	kink
terminology	S1	S2	C3	C5	D	K
number of atoms	72	72	156	210	88	116
dimension[a] (Å) along the						
x-axis	6.73	6.02	6.73	6.73	9.02	9.02
y-axis	12.76	12.76	17.01	21.27	12.76	17.01
z-axis: vacuum thickness	16.5	16.5	16.5	16.5	16.5	16.5
slab thickness	7.44	9.02	15.04	15.04	9.92	9.92
projected surface areas A (Å^2)	85.83	76.77	153.53	191.91	85.83	114.44
k points mesh	2 × 2 × 1	2 × 2 × 1	2 × 1 × 1	2 × 1 × 1	2 × 2 × 1	2 × 2 × 1
surface energy Γ (J·m^{-2}) after relaxation	1.56	1.77	3.00	2.78	1.89	2.66

[a] $d_{Mg-O} = 2.127$ Å for unrelaxed systems (calculated by energy minimization on MgO bulk).

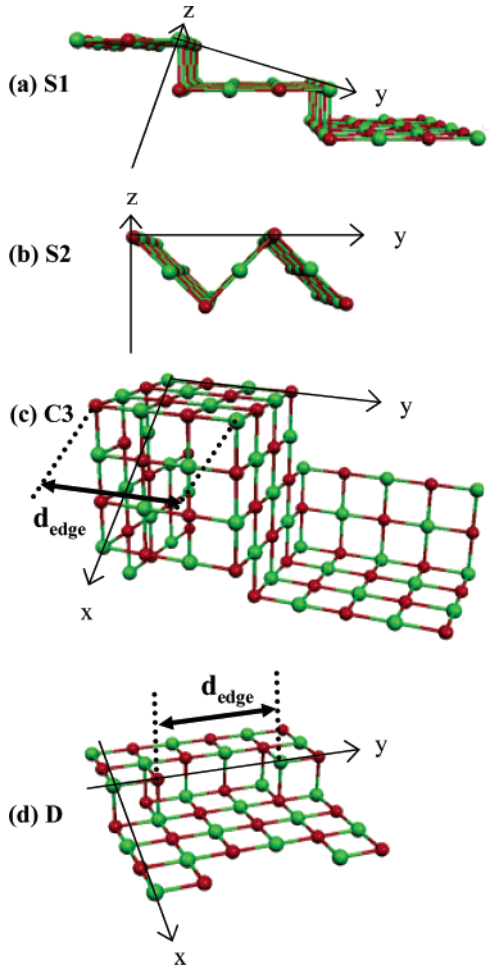

Figure 2. Structure of the simulated systems before relaxation (outermost layer only) and periodicity axes: (a) monatomic step S1, side view; (b) diatomic step S2, side view; (c) corners C3, perspective view; (d) step divacancy D, perspective view. In each case, the lacking axis completes the direct (x, y, z) trihedra. The corners C5 and kinks K systems are oriented in the same way as C3 and D, respectively. The O and Mg atoms of the surface are represented by red and green spheres, respectively.

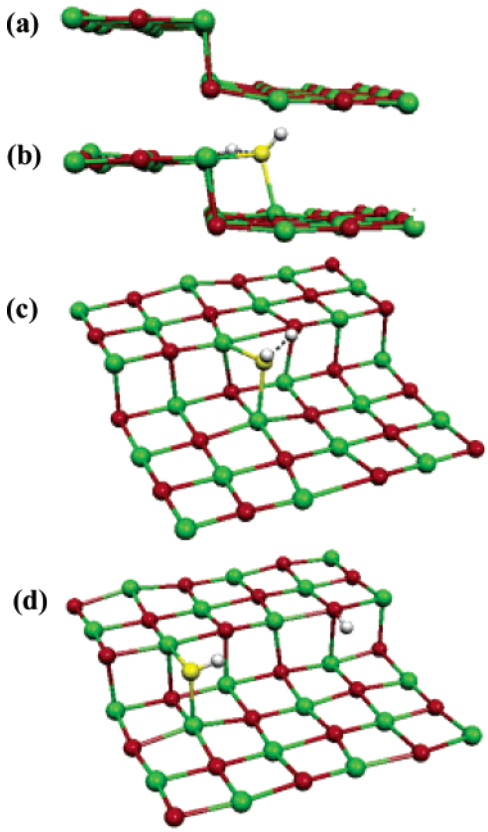

Figure 3. Outermost layer of the monatomic step S1: (a) dehydrated and relaxed (side view); (b) and (c) monohydrated and hydrogen-bonded S1−1w−H (side and perspective views respectively); (d) monohydrated and not hydrogen-bonded S1−1w−nH (perspective view). H and O coming from water molecules are drawn as white and yellow spheres, respectively.

Mg_{3C}, respectively (see Supporting Information). For $n_{ads} = 2$, the water molecules are adsorbed parallel to the edge linking the corners, (C3−2w−side) or face to face, perpendicular to the edge (C3−2w−front). A similar terminology is adopted for C5. For D, four different configurations of D−1w are considered, called D−1w−Mg_{3C}−O_{3C}, D−1w−Mg_{3C}−O_{4C}, D−1w−Mg_{3C}−O_{5C}, and D−1w−Mg_{4C}−O_{3C} to indicate the coordination of the hydroxylated $Mg^{2+}{}_{LC}$ and the protonated $O^{2-}{}_{L'C}$ (see Figure 5). A similar nomenclature is used for K. However, due to the long distance between $Mg^{2+}{}_{3C}$ and $O^{2-}{}_{3C}$ in K, their respective hydroxylation and protonation by a single water molecule is unlikely, so that K−1w−Mg_{3C}−O_{3C} is not studied.

2.3. Thermodynamics. The hydration energy per water molecule is calculated at 0 K thanks to eq 2, where U^{hyd}_{relax}, U^{dehyd}_{relax}, and U_{water} are the energies of the relaxed hydrated system, of the relaxed dehydrated system, and of the water molecule, respectively. n_{ads} stands for the number of water molecules per supercell.

$$\Delta_{hyd}U_{(0K)} = \frac{1}{n_{ads}}\left(U^{hyd}_{relax(0K)} - U^{dehyd}_{relax(0K)} - n_{ads}U_{water(0K)}\right) \quad (2)$$

Following the formalism developed for alumina and titania

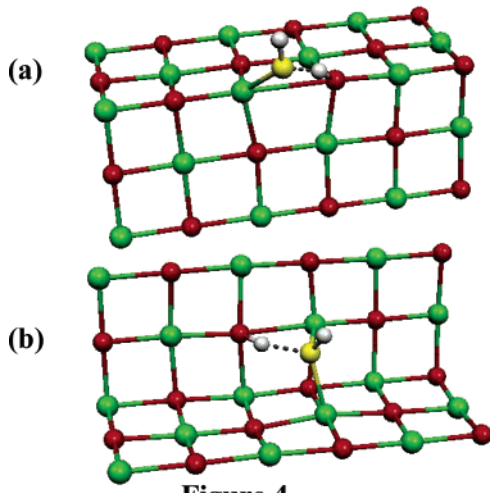

Figure 4

Figure 4. Perspective views of the outermost layer of the monohydrated diatomic step S2: (a) S2−ON−1w and (b) S2−IN−1w.

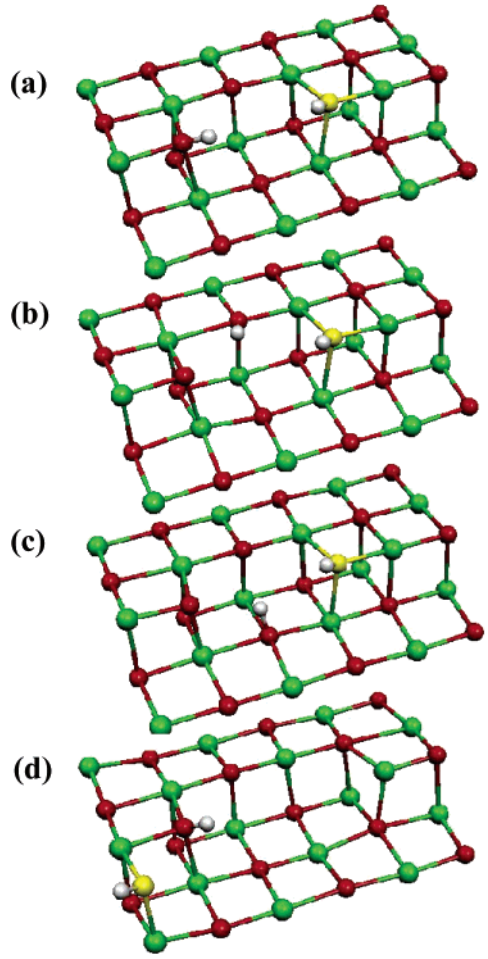

Figure 5. Perspective views of the various configurations for the outermost layer of the hydrated step divacancies D: (a) D−1w−Mg_{3C}−O_{3C}, (b) D−1w−Mg_{3C}−O_{4C}, (c) D−1w−Mg_{3C}−O_{5C}, and (d) D−1w−Mg_{4C}−O_{3C}.

surfaces,[31,32,56] the surface Gibbs energy $\Gamma_{(T)}$ can be expressed as follows, provided that entropic and PV terms are neglected for condensed phases

$$\Gamma_{(T)} = \Gamma_{dry(T)} + \frac{\theta_{OH}}{2}\Delta_{hyd}G_{(T)} \quad (3)$$

Γ_{dry} is the surface energy of the fully dehydrated system, θ_{OH} the coverage by hydroxyls, and $\Delta_{hyd}G$ the hydration molar Gibbs energy, for a single water molecule. Equation 3 can be rewritten as follows

$$\Gamma_{(T)} = \Gamma_{(0K)} + \frac{\theta_{OH}}{2}\left[TS^{\circ}_{(T)} - H^{\circ}_{(T)} + H^{\circ}_{(0K)} - kT\ln\left(\frac{P}{P^{\circ}}\right)\right] \quad (4)$$

H° and S° are the standard enthalpy and entropy of the water molecule respectively, calculated thanks to Gaussian 03.[57] The pressure P was fixed to be 10^{-2} Pa, typical for experiments performed with powders.[30]

3. Results

3.1. Geometries and Surface Energies of Dehydrated Surfaces. Dehydrated systems exhibit a noticeable relaxation compared with the ideal cubic geometry, especially for the lowest coordinated ions, as illustrated for S1 in Figure 3a.

The ($O_{4C}Mg_{6C}O_{5C}$) and ($Mg_{4C}O_{6C}Mg_{5C}$) angles increase up to 17% (103.5° and 105.6°, respectively, vs 90° in the unrelaxed system). Surface Mg−O distances are decreased up to 3% upon relaxation, especially around $Mg^{2+}{}_{4C}$. Mg_{LC}−$O_{L'C}$ distances are even more reduced (up to 12%) for L or L′ = 3, for the corner systems and for the step vacancies. This indicates that the driving force for the surface relaxation is the lack of coordination, as confirmed by higher surface energies for systems containing 3C ions (Table 1). In each case (C3/C5, K, D), the relaxation is stronger in the vicinity of $Mg^{2+}{}_{3C}$ than of $O^{2-}{}_{3C}$. This may be due to the larger polarizability of O^{2-} (ionic radius, $r(O^{2-}) = 1.40$ Å, $r(Mg^{2+}) = 0.72$ Å), which enables an easier relaxation of the electronic density compared with Mg^{2+}, as already suggested by Susko et al.[58] These defects are all metastable compared with the (100) plane ($\Gamma = 1.10$ J·m^{-2} [59]).

3.2. Geometries of Hydrated Systems at 0 K. The surface lattice geometry is markedly influenced by hydration. Parts b−d of Figure 3 depict the relaxed structures of S1−1w−H and S1−1w−*n*H. Hydration tends to restore locally the ideal lattice angle. The distance between the adsorbing $Mg^{2+}{}_{4C}$ and $O^{2-}{}_{4C}$ increases markedly (31%) to allow for stabilization of the hydroxyls by hydrogen bonding. This distortion decreases as the number of adsorbed molecules increases (3% for S1−3w). This is also noticed for S2−IN and S2−ON. At high coverage, the lateral relaxation of the surface site is constrained by that of the neighbors, hence relaxation is less efficient.

The adsorbed water molecules dissociate in any case studied, but the geometry of the hydroxyls depends on their location. On S1, as expected, O_{4C}−H species are formed upon protonation of $O^{2-}{}_{4C}$ of the edge. However, instead of the expected monocoordinated O_{1C}−H groups, hydroxylation of $Mg^{2+}{}_{4C}$ provides dicoordinated O_{2C}−H groups, insofar as bridging to the $Mg^{2+}{}_{5C}$ belonging to the underlying (100) plane occurs. Bridging is no longer observed on the edge of the higher step (Figure 4a, S2−ON−1w).

On the edge of S2, the water molecules are in a less dissociated state than on S1. The expected O_{4C}−H and O_{1C}−H formed on S2 remain strongly hydrogen bonded (hydrogen-bond lengths, 1.432 Å for S2−ON−1w vs 1.827 Å for S1−1w−H). In the valley of S2 (Figure 4b, case of S2−IN−1w), bridging occurs between two $Mg^{2+}{}_{5C}$, resulting in the formation of O_{2C}−H groups, as well as O_{5C}−H. They interact via hydrogen bonding but more weakly than on S2−ON (hydrogen-bond length, 1.559 Å for S2−IN−1w).

TABLE 2: Hydration Energy $\Delta_{hyd}U$ (kJ·mol^{-1}) Per Water Molecule for the Surface Defects Modeled for MgO

steps	ions involved	−1w−nH	−1w−H	−2w	−3w
S1−	Mg^{2+}_{4C}, Mg^{2+}_{5C}, O^{2-}_{4C}	−93	−194	−174	−168
S2−ON	Mg^{2+}_{4C}, O^{2-}_{4C}	not studied	−143	−121	−111
S2−IN	Mg^{2+}_{5C}, Mg^{2+}_{5C}, O^{2-}_{5C}	not studied	−103	−100	−99
corners		−1w−O_{3C}	−1w-Mg_{3C}	−2w-side	−2w-front
ions involved		Mg^{2+}_{4C}, O^{2-}_{3C}	Mg^{2+}_{3C}, O^{2-}_{4C}	Mg^{2+}_{4C}, Mg^{2+}_{3C}, O^{2-}_{3C}, O^{2-}_{4C}	Mg^{2+}_{4C}, Mg^{2+}_{3C}, O^{2-}_{3C}, O^{2-}_{4C}
C3−		−168	−155	−159	−153
C5−		−173	−154	−162	−154
step vacancies		−1w−Mg_{3C}-O_{3C}	−1w−Mg_{3C}-O_{4C}	−1w−Mg_{3C}−O_{5C}	−1w−Mg_{4C}−O_{3C}
ions involved		Mg^{2+}_{3C}, Mg^{2+}_{4C}, Mg^{2+}_{5C}, O^{2-}_{3C}	Mg^{2+}_{3C}, Mg^{2+}_{4C}, Mg^{2+}_{5C}, O^{2-}_{4C}	Mg^{2+}_{3C}, Mg^{2+}_{4C}, Mg^{2+}_{5C}, O^{2-}_{5C}	Mg^{2+}_{4C}, Mg^{2+}_{5C}, O^{2-}_{3C}
D−		−372	−322	−264	−241
K−		not studied	−260	−235	−248

Hydrated C3 and C5 geometrically behave quite similarly. The surface lattice is distorted upon water adsorption, resulting in elongation of the Mg_{3C}−O_{4C} (+26%) or Mg_{4C}−O_{3C} (+34%) distances involved in adsorption (see Supporting Information for C3). The expected O_{1C}−H, O_{3C}−H, and O_{4C}−H are obtained, because no bridging is possible on a corner at the intersection of extended edges.

D and K exhibit similar hydrated configurations with isolated hydroxyls (Figure 5 for D).

Each time that hydroxylation of the Mg^{2+}_{3C} ions is involved, the hydroxyl partially fills the vacancy, bridging 3 Mg^{2+}_{LC} (Mg^{2+}_{3C}, Mg^{2+}_{4C}, and Mg^{2+}_{5C}) leading to a O_{3C}−H. D−1w−Mg_{3C}−O_{3C} thus exhibits two equivalent O_{3C}−H groups. D−1w−Mg_{4C}−O_{3C} and K−1w−Mg_{4C}−O_{3C} contain isolated O_{2C}−H and O_{3C}−H.

3.3. Hydration Energies at 0 K. Upon hydration, the MgO surface is always stabilized, as shown by the negative values for the hydration energies (Table 2). Hydrogen bonding seems to prevent migration of the proton along the step as shown by the much stronger interaction of water (up to 101 kJ·mol^{-1}) for S1−1w−H than for S1−1w−*n*H. Within the hydrogen-bonded configurations, an increase of the number of adsorbed water molecules leads to an increase in $\Delta_{hyd}U$ (negative values) for S1 and S2 (IN and ON independently). This can be tentatively assigned to the stabilizing elongation of the Mg_{4C}−O_{4C} distance mentioned in section 3.2, after water adsorption, which is less efficient at high coverage, or to the influence of water adsorption on the Madelung potential at neighboring sites. For C3 and C5 on the contrary, $\Delta_{hyd}U$ remains almost unchanged upon increased water content, which can be linked to the ability of the corners to adapt independently their geometry to water adsorption. The comparison of C3−2w−side and C3−2w−front shows that water molecules are stabilized by adsorption on the same edge, probably upon dipolar interaction. The relative $\Delta_{hyd}U$ values for C3−1w−O_{3C} and C3−1w−Mg_{3C} reveal a slightly stronger interaction of water with a corner terminated by O^{2-}_{3C} than by Mg^{2+}_{3C}. For the various hydration configurations of D and K, keeping constant the coordination of the adsorbing Mg^{2+}, $\Delta_{hyd}U$ decreases with the coordination of the protonated oxide ion. The same decrease occurs by fixing the coordination of the protonated oxide ion and decreasing the coordination of the hydroxylated cation.

From one system to another, focusing on the nature of the defect and on the adsorption of a single water molecule in the most stable configuration, the following order is observed for the hydration energy: S2−IN < S2−ON < C3 ≈ C5 < S1 < K < D. Indeed, water interacts more strongly with systems enabling bridging of OH^- (S1, K, and D) than with C3, C5, and especially S2 where no bridging is possible.

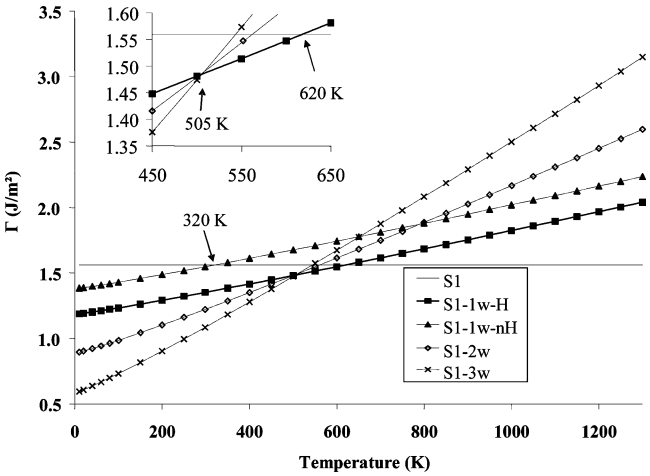

Figure 6. Surface free energy as a function of temperature for S1, at a pressure of 10^{-2} Pa, with several coverages of the step. Inset: extended view of the crossing region.

3.4. Thermodynamic Properties. Surface energies are calculated as a function of temperature for $P = 10^{-2}$ Pa. The case of S1 is shown in Figure 6, which indicates that S1−3w is the most stable system up to about 500 K, S1−1w−H from 500 to 620 K, and dehydrated S1 above 620 K. As expected from hydration energies values, S1−1w−*n*H is never the most stable system. This also seems to be the case for S1−2w.

The same kind of diagram has been drawn for each system, and the thermal stabilities are deduced. Not physically significant systems, such as S1−1w−*n*H, which does not exhibit the lowest surface energy for a given number of water molecules, are discarded. S2−IN and S2−ON are however both mentioned, as the first one is expected to model the behavior of the valley of high steps, whereas the second one depicts the trend followed by their edge. C3/C5−1w−O_{3C} and C3/C5−1w−Mg_{3C} model independently adsorptions on O^{2-}_{3C} and Mg^{2+}_{3C}-terminated corners and as a consequence have to be both considered. C5 also models the behavior of cubic nanoparticles toward water. D is the simulation of a single system, which the most stable hydration configuration is D−1w−Mg_{3C}−O_{3C}. K depicts at the same time O^{2-}_{3C} and Mg^{2+}_{3C}-terminated kinks, existing inde-

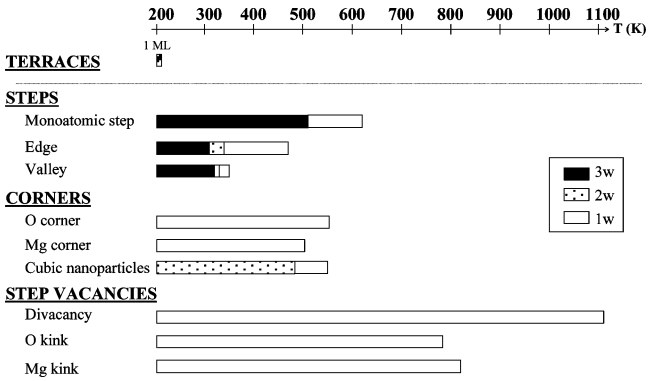

Figure 7. Thermal stability domains of hydrated systems for $P = 10^{-2}$ Pa. The behavior of the terraces is inferred from their hydration energy given in the literature[11] and eq 5. Results on monatomic steps, edges, and valleys come from S1, S2−ON, and S2−IN, respectively. Thermal stabilities given for the O and Mg corners are inferred from C3/C5−1w−O_{3C} and C3/C5−1w−Mg_{3C}, respectively (C3 and C5 provide almost the same results). C3 and C5 account for the behavior of cubic nanoparticles. Hydration of divacancies, O kinks, and Mg kinks are depicted by the behavior of D−1w−Mg_{3C}−O_{3C}, K−1w−Mg_{4C}−O_{3C}, and K−1w−Mg_{3C}−O_{4C}, respectively.

pendently on the real MgO surface. K−1w−Mg_{4C}−O_{3C} will thus be studied next, despite that it is less stable than K−1w−Mg_{3C}−O_{4C}. Moreover, the phenomenological law has been found for the dehydration temperature T_d

$$T_d = \frac{\Delta_{hyd}U - B}{R\ln(P/P^\circ) + A} \qquad (5)$$

with $A = -0.208$ kJ·mol^{-1}·K^{-1} and $B = 11.684$ kJ·mol^{-1} which enables us to infer T_d for MgO(100) covered by a water monolayer. By the use of the calculated value[11] $\Delta_{hyd}U = -58$ kJ·mol^{-1}, in very good agreement with the experimental one,[60] $T_d = 204$ K is obtained.

The thermal stabilities of the physically significant systems are reported in Figure 7. The loss of H_2 from D−1w−Mg_{3C}−O_{3C} has moreover been studied, but it is strongly endoenergetic (558.5 kJ·mol^{-1}) so that the dehydration (involving $-\Delta_{hyd}U =$ 372 kJ·mol^{-1}) is more favored than the dehydrogenation.

4. Discussion

It can be noticed that the C3 and C5 systems behave quite similarly, indicating that the C3 system is large enough to provide accurate description of $O^{2-}{}_{3C}$ and $Mg^{2+}{}_{3C}$-terminated corners.

4.1. Water Dissociation on MgO: Concave vs Convex Systems. It can be observed from hydration energies (Table 2) that S1 interacts more strongly with water than C3/C5, as already observed on CaO.[61] The coordination of the ions (3C in the latter, 4C in the former) is hence not the only factor controlling the strength of water adsorption. In fact, on S1, OH groups formed upon hydroxylation of $Mg^{2+}{}_{4C}$ interact also with $Mg^{2+}{}_{5C}$ of the underlying terrace, becoming O_{2C}−H. This supplementary interaction explains the stronger hydration energy (by more than 50 kJ·mol^{-1}) compared with the diatomic step. This is even more pronounced in $Mg^{2+}{}_{3C}$-terminated kinks and step divacancies where the expected O_{1C}−H becomes O_{3C}−H, giving rise to a much stronger interaction (up to 168 kJ·mol^{-1}) than that for $Mg^{2+}{}_{3C}$-terminated corners. More generally, this is the case for concave areas (Figure 8), for example, surface portions where curvature is centered outside the surface, such as S1, S2−IN, D, and K. On the contrary, convex areas such as S2−ON and C3/C5 do not enable bridging. This notion of concave/convex area meets the proposition of inverse corners as preferred sites for H_2 dissociation, reported in the literature by combined experimental and theoretical approaches.[62−65]

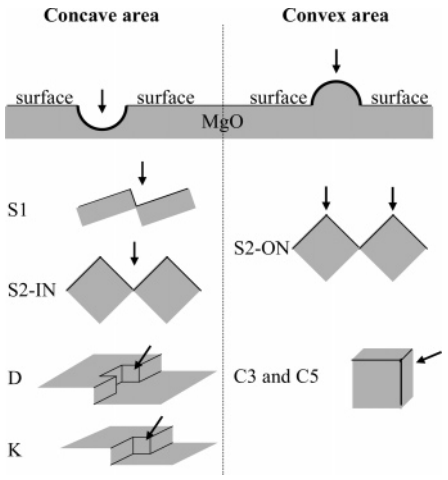

Figure 8. Schematized representation of concave and convex areas: general case (top) and examples. Arrows depict the surface area where water adsorption takes place.

It can be noticed that bridging on monatomic steps and in valleys has already been mentioned on MgO and CaO[26,61] and that the missing oxide ion in oxygen vacancies[13] and terrace divacancies[34] is filled by the water oxygen atom, as observed here for D. The determining role of bridging is also supported by calculations of Abdel Halim et al.[29] and Gay et al.[66] on MgO-(110). The former authors constrain the geometry of hydroxyls, preventing any bridging, while the latter allow the possibility of bridging, leading to a very strong stabilization, although the term of bridging is not used in their paper.

Inside each category (concave and convex), the presence of 3C ions is correlated with a stronger interaction with water. This can be linked to the higher energy of the fundamental level as coordination numbers decrease.[58,67,68] The first-order parameter for water adsorption strength on MgO is thus the bridging of OH groups in concave areas, with the second-order factor being ion coordination.

4.2. Link with Acido-basicity. A relation thus exists between the strength of the interaction with water and the local topology of the surface. A deeper analysis can be performed to rationalize the acido-basicity of surface ions. In the water adsorption process, the molecule is dissociated: the Brønsted basicity of the surface, defined as the ability for a species to protonate itself, is thus involved. On the MgO surface, it is characterized by the deprotonation equilibrium constant relative to eq 1, written for the case of H_2O but valid for any species of the type RH with R^- replacing OH^-. The Brønsted basicity of the Mg^{2+}−O^{2-} pair thus depends at the same time on the deprotonating ability of O^{2-}, and of the Lewis acidity of the Mg^{2+} toward the remaining HO^-. The Brønsted basicity of an oxide ion corresponds in this case to its Lewis basicity toward a proton. The deprotonation equilibrium is equivalent to the hydration one; hydration energies $\Delta_{hyd}U$ (that can be approximated at 0 K to $\Delta_{hyd}G$) thus give a direct insight into the Brønsted basicity.

Since only systems hydrated with a single water molecule are considered in section 4.2, the "1w" indication is omitted in what follows. The divacancy will moreover be set apart from the other systems for the reasoning on coordination as it has been shown by Pisani and co-workers[55] that it provides a peculiar electrostatic field accounting for strong interactions with protic molecules.

From Table 2, the systems studied can be classified from the less to the most basic toward water in the following sequence

$$S2-IN < S2-ON < C3-Mg_{3C} < C3-O_{3C} < S1 < K-Mg_{3C}-O_{5C} < K-Mg_{4C}-O_{3C} < K-Mg_{3C}-O_{4C}$$

For the divacancy D, the various configurations can also give rise to comparison, insofar as the electrostatic environment is kept the same: $D-Mg_{4C}-O_{3C} < D-Mg_{3C}-O_{5C} < D-Mg_{3C}-O_{4C} < D-Mg_{3C}-O_{3C}$. Taking into account all the surface ions involved in water dissociation, these classifications provide inequalities linking the deprotonating/stabilizing abilities of the surface $O^{2-}{}_{L'C}$ and $Mg^{2+}{}_{LC}$, respectively. For example, the classification, S2−IN < S2−ON, can be translated in: $2Mg^{2+}{}_{5C} + O^{2-}{}_{5C} < Mg^{2+}{}_{4C} + O^{2-}{}_{4C}$. Information on the relation between coordination and acido-basicity can thus be deduced.

4.2.1. Coordination and Basicity of $O^{2-}{}_{L'C}$ Ions. From the comparison of S2−ON and $C3-O_{3C}$ on one hand, and of $K-Mg_{3C}-O_{5C}$ and $K-Mg_{3C}-O_{4C}$ on the other hand, the following order of deprotonating ability is obtained: $O^{2-}{}_{5C} < O^{2-}{}_{4C} < O^{2-}{}_{3C}$. The same order is provided from the comparison of $D-Mg_{3C}-O_{5C}$, $D-Mg_{3C}-O_{4C}$, and $D-Mg_{3C}-O_{3C}$. For the same stabilization (one or several Mg^{2+}), the Brønsted basicity of an oxide ion increases when its coordination decreases. The same kind of inequalities can be written using the adsorption energies calculated in the case of methanol dissociation on terraces, edges, and corners[69] and in the case of acetylene for $O^{2-}{}_{4C}$ and $O^{2-}{}_{3C}$.[70] This is linked to a reduced Madelung potential for low-coordinated ions.

This is confirmed by experimental and theoretical studies of the adsorption of Lewis acid entities other than the proton. CO_2 has been very often used experimentally to quantify the number and strength of basic sites on MgO. However, numerous adsorption modes evidenced theoretically[71] lead to complex IR features[72,73] and composite TPD profiles,[6,72−74] so that the assignment in terms of ion coordination have never been proposed. Recently, BF_3 adsorption on MgO has been theoretically proposed as an accurate probe molecule to evaluate the basicity of oxide ions,[75] as the adsorption energy increases as the coordination of the adsorbing oxide ion decreases. Additional information is provided by the theoretical study of adsorbed metal atom on MgO:[76] the interaction is favored on $O^{2-}{}_{L'C}$ of lowest coordination.

4.2.2. Coordination and Lewis Acidity of $Mg^{2+}{}_{LC}$ Ions. From the comparison of S2−ON and $C3-Mg_{3C}$, the ability for a magnesium cation to stabilize the remaining hydroxyl increases in the following order: $Mg^{2+}{}_{4C} < Mg^{2+}{}_{3C}$. No evidence is given here for the relative stabilizing ability of $Mg^{2+}{}_{5C}$. The same result can be inferred by transposing the method followed here to adsorption energies calculated for acetylene[70] and methanol dissociation.[69]

This can be compared with the adsorption of CO, selective probe molecules for Lewis acidic sites, reported in the literature. Its adsorption at 77[77,78] and 20 K[79] leads to molecular adsorption on Mg^{2+}. IR shifts, adsorption enthalpies measurements, and theoretical calculations[80−84] indicate that the Lewis acidity of $Mg^{2+}{}_{LC}$ increases when its coordination decreases, in agreement with the present work.

4.2.3. Ion Pairs Coordination and Brønsted Basicity Toward Water. As a consequence of the relative basicity/acidity of 4C and 3C ions and of the comparison of S2−IN and S1, the trend for deprotonation follows: $Mg^{2+}{}_{5C} + O^{2-}{}_{5C} < Mg^{2+}{}_{4C} + O^{2-}{}_{4C} < Mg^{2+}{}_{3C} + O^{2-}{}_{3C}$. The theoretical study of the adsorption of other protic molecules[69,70,85] supports this result.

Furthermore, the comparison of $C3-Mg_{3C}$ with $C3-O_{3C}$ indicates that $Mg^{2+}{}_{3C} + O^{2-}{}_{4C} < Mg^{2+}{}_{4C} + O^{2-}{}_{3C}$, which tends to show that the coordination of O^{2-} influences the Brønsted basicity of an $Mg^{2+}-O^{2-}$ pair toward water more strongly than the coordination of Mg^{2+}. The amplitude of this effect is however small, as shown by similar values obtained for $\Delta_{hyd}U$. It is therefore not surprising to notice contradictory results in the literature upon protic molecules dissociation, with some of them being in line with the dominating effect of oxygen[86] others not.[69,70] Artifacts induced by the level of the calculations may have a higher amplitude than the real chemical effect, so that no definitive conclusion can be stated now.

4.2.4. Cooperative Effect between Several Ions Leading to an Increase of Basicity. As mentioned previously, the existence of the lowest coordinated ions does not automatically lead to the strongest interaction with water. Bridging of hydroxyls between several Mg^{2+} appears as a key factor that can invert expected orders, as illustrated by the comparisons of $C3-O_{3C}$ and S1, giving, $O^{2-}{}_{3C} < O^{2-}{}_{4C} + Mg^{2+}{}_{5C}$ and $C3-Mg_{3C}$ and S1, leading to, $Mg^{2+}{}_{3C} < Mg^{2+}{}_{4C} + Mg^{2+}{}_{5C}$. Thus, the basicity of $O^{2-}{}_{4C}$ can be increased by the additional stabilization provided by $Mg^{2+}{}_{5C}$, to such an extent that they become together more basic than a single $O^{2-}{}_{3C}$. This cooperation also influences the Lewis acidity of $Mg^{2+}{}_{3C}$, exceeded by the combined Lewis acidity of several $Mg^{2+}{}_{LC}$ of higher coordination. This cooperation effect of several Mg^{2+} cannot be easily evidenced for O^{2-} in the case of water because of the difficulty for a proton to bridge several oxide ions. It has however been theoretically observed for a rhodium atom on monatomic steps,[76] bridging an $O^{2-}{}_{4C}$ and an $O^{2-}{}_{5C}$, more favorably than on an $O^{2-}{}_{3C}$ corner, so that as follows: $O^{2-}{}_{3C} < O^{2-}{}_{4C} + O^{2-}{}_{5C}$. The $O^{2-}{}_{5C}$ ion thus cooperates with the basicity of $O^{2-}{}_{4C}$, and vice versa, to dominate over the basicity of $O^{2-}{}_{3C}$.

As a conclusion, the MgO surface exhibiting the highest possible Brønsted basicity can be obtained by increasing at the same time the content of 3C ions and the bridging abilities when the R^- moiety of the protic molecule is able to be bridged. This can explain why cubic particles deprotonate a lower quantity of methanol per surface area compared with an MgO powder obtained by sol−gel routes, exhibiting at the same time a high proportion of $O^{2-}{}_{3C}$ ions and an irregular surface.[1]

The case of water as the protic molecule has been studied. Differences between probe molecules are however to be expected, depending on the ability of the R^- moiety to bridge several $Mg^{2+}{}_{LC}$: for example, the ability of CO to bridge one $Mg^{2+}{}_{4C}$ and one $Mg^{2+}{}_{5C}$ has been evidenced by theoretical calculations[83] but it leads to weaker interaction than with a single $Mg^{2+}{}_{3C}$, probably because of large distances between the carbon of CO and bridged Mg^{2+}. The role of oxygen (existing in the case of water through its HO^-, vs carbon in the case of CO) in bridging seems to be of significant importance.

4.3. State of the Surface at Increasing Temperature. Figure 7 provides a description of the state of the surface at increasing temperature for $P = 10^{-2}$ Pa. The calculated desorption temperature $T_d = 204$ K for MgO(100) is in quite good agreement with experimental desorption at about 250 K under evacuation at about 3×10^{-8} Pa.[18,21,87,88] Once clean terraces are recovered, valleys are dehydrated, at about 350 K. Water on the edge of high steps begins to desorb, but their full dehydration is achieved at 475 K. $Mg^{2+}{}_{3C}$-terminated corners are then dehydrated at 500 K; $O^{2-}{}_{3C}$-terminated corners are at 550 K. Desorption from the corners starts within the same temperature window as the partial dehydration of monatomic steps, which is complete only at higher temperature (620 K).

O^{2-}_{3C} and Mg^{2+}_{3C}-terminated kinks are then successively dehydrated (740 and 805 K); water thus only remains on step divacancies. The highest desorption temperature calculated is 1110 K.

Information on other surface defects exists in the literature. Oxygen vacancies on terraces interact strongly with water, but H_2 desorption is expected on this surface site instead of dehydration.[13] Our calculations show that H_2 desorption is not expected from step divacancies. From the literature, divacancies on terraces are partially healed by water, like oxygen vacancies and step divacancies.[34] Their interaction with water is strong, so that they may contain hydroxyls at rather high temperature.

Entropic effects for the condensed phase are neglected in our thermodynamic approach, which could have an influence especially at high temperature. Kinetic effects could also play a role. Electrostatic investigation of surface defects is in favor of spontaneous dissociation of protic molecules in monatomic steps and divacancies,[55] but to our knowledge, no data is available on kinetic limitations of the thermal desorption process on MgO. It was recently theoretically shown that there is no additional barrier for water desorption from Al_2O_3, besides the reaction endothermicity.[89] Moreover, thermal diffusion of adsorbed species could occur at high temperatures, which has not been taken into account.

5. Conclusion

Low-coordinated ions on MgO, on mono- and diatomic steps (exhibiting Mg^{2+}_{4C} and O^{2-}_{4C}), on corners, kinks, and step divacancies (with O^{2-}_{3C} and Mg^{2+}_{3C}) have been modeled thanks to periodic DFT calculations. The strength of the interaction of MgO with water has been evaluated thanks to hydration energies. Systems exhibiting only 5C ions as adsorbing sites (valley of high steps) interact weakly with water. For all other systems, two factors control the hydration thermodynamics: the concave nature of the surface, which enables bridging of the hydroxyls to surface Mg^{2+}, and the ion coordination. Indeed, contrary to the expected monocoordinated hydroxyls, dicoordinated OH groups are formed on monatomic steps and in the valleys and $O_{3C}-H$ species appear in step divacancies and Mg^{2+}_{3C}-terminated kinks. Inside each system category (concave/convex), 3C ions provide stronger interaction than 4C ions.

A thermodynamic basicity (of $O^{2-}_{L'C}$) and acidity (of Mg^{2+}_{LC}) ranking is proposed on the basis of hydration energy. The Lewis basicity and acidity of O^{2-}_{LC} and Mg^{2+}_{LC}, respectively, increase as their coordination decreases. The same trend is followed by the Brønsted basicity of the $Mg^{2+}_{LC}-O^{2-}_{L'C}$ pair. However, this trend can be reversed when bridging occurs, involving the cooperative effect of several Mg^{2+}, with an important implication on the role of surface morphology on the basicity of MgO samples. A description of the state of the hydrated surface as a function of evacuation temperature for $P = 10^{-2}$ Pa is proposed on the basis of thermodynamic calculations, taking into account entropic effects in the gas phase. The most striking result is that the corners are dehydrated at lower temperature than the monatomic steps, due to the cooperative effect of the magnesium cations in the latter case.

Acknowledgment. The authors wish to express their gratitude to Hélène Lauron-Pernot and Dominique Costa from Laboratoire de Réactivité de Surface for very interesting discussions. Most of the calculations were carried out at the CNRS-IDRIS computational center (Orsay, France), under Project No. 051847.

Supporting Information Available: Figure showing the side views of the outermost layer of the hydrated corners of C3. This material is available free of charge via the Internet at http://pubs.acs.org.

References and Notes

(1) Bailly, M. L.; Chizallet, C.; Costentin, G.; Krafft, J. M.; Lauron-Pernot, H.; Che, M. *J. Catal.* **2005**, *235*, 413−422.
(2) Knözinger, E.; Jacob, K. H.; Hofmann, P. *J. Chem. Soc., Faraday Trans.* **1993**, *89*, 1101−1107.
(3) Anpo, M.; Yamada, Y.; Kubokawa, Y. *J. Chem. Soc., Chem. Commun.* **1986**, *9*, 714−716.
(4) Zhang, G.; Hattori, H.; Tanabe, K. *Appl. Catal.* **1988**, *36*, 189−197.
(5) Wang, J. A.; Bokhimi, X.; Novaro, O.; Lopez, T.; Gomez, R. *J. Mol. Catal. A: Chem.* **1999**, *145*, 291−300.
(6) Kus, S.; Otremba, M.; Torz, A.; Taniewski, M. *Fuel* **2002**, *81*, 1755−1760.
(7) Hoq, M. F.; Nieves, I.; Klabunde, K. J. *J. Catal.* **1990**, *123*, 349−363.
(8) Boudart, M.; Delbouille, A.; Derouane, E. G.; Indovina, V.; Walters, A. B. *J. Am. Chem. Soc.* **1972**, *94*, 6622−6630.
(9) Parker, S. C.; De Leeuw, N. H.; Redfern, S. E. *Faraday Discuss.* **2000**, *114*, 381−393.
(10) Che, M.; Tench, A. J. *Adv. Catal.* **1982**, *31*, 77−133 and AERE Report-R9971, Nov. 1980.
(11) Giordano, L.; Goniakowski, J.; Suzanne, J. *Phys. Rev. Lett.* **1998**, *81*, 1271−1273.
(12) Odelius, M. *Phys. Rev. Lett.* **1999**, *82*, 3919−3922.
(13) Finocchi, F.; Goniakowski, J. *Phys. Rev. B* **2001**, *64*, 125426, 1−8.
(14) Sitte, L. D.; Alavi, A.; Lynden-Bell, R. M. *J. Chem. Phys.* **2000**, *113*, 3344−3350.
(15) Lynden-Bell, R. M.; Sitte, L. D.; Alavi, A. *Surf. Sci.* **2002**, *496*, L1−L6.
(16) Kim, Y. D.; Lynden-Bell, R. M.; Alavi, A.; Stultz, J.; Goodman, D. W. *Chem. Phys. Lett.* **2002**, *352*, 318−322.
(17) Giordano, L.; Goniakowski, J.; Suzanne, J. *Phys. Rev. B* **2000**, *62*, 15406−15408.
(18) Kim, Y. D.; Stultz, J.; Goodman, D. W. *J. Phys. Chem. B* **2002**, *106*, 1515−1517.
(19) Yu, Y.; Guo, Q.; Wang, E.; Möller, P. J. *Phys. Rev. B* **2003**, *68* (1−4), 115414.
(20) Stimiman, M. J.; Huang, C.; Scott Smith, R.; Joyce, S. A.; Kay, B. D. *J. Chem. Phys.* **1996**, *105*, 1295−1298.
(21) Ahmed, S. I.; Perry, S. S.; El-Bjeirami, O. *J. Phys. Chem. B* **2000**, *104*, 3343−3348.
(22) Liu, P.; Kendelewicz, T.; Brown, G. E. J.; Parks, G. A. *Surf. Sci.* **1998**, *412/413*, 287−314.
(23) Liu, P.; Kendelewicz, T.; Brown, G. E. J. *Surf. Sci.* **1998**, *412/413*, 315−332.
(24) Scamehorn, C. A.; Harrison, N. M.; Carthy, M. I. M. *J. Chem. Phys.* **1994**, *101*, 1547−1554.
(25) Langel, W.; Parrinello, M. *J. Chem. Phys.* **1995**, *103*, 3240−3252.
(26) De Leeuw, N. H.; Watson, G. W.; Parker, S. C. *J. Phys. Chem.* **1995**, *99*, 17219−17225.
(27) Almeida, A. L.; Martins, J. B. L.; Taft, C. A.; Longo, E.; Andres, J.; Lie, S. K. *J. Mol. Struct. (THEOCHEM)* **1998**, *426*, 199−205.
(28) Tikhomirov, V. A.; Geudtner, G.; Jug, K. *J. Mol. Struct. (THEOCHEM)* **1999**, *458*, 161−169.
(29) Abdel Halim, W. S.; Shalabi, A. S. *Appl. Surf. Sci.* **2004**, *221*, 53−61.
(30) Knözinger, E.; Jacob, K. H.; Singh, S.; Hofmann, P. *Surf. Sci.* **1993**, *290*, 388−402.
(31) Digne, M.; Sautet, P.; Raybaud, S.; Euzen, P.; Toulhoat, H. *J. Catal.* **2004**, *226*, 54−68.
(32) Arrouvel, C.; Digne, M.; Breysse, M.; Toulhoat, H.; Raybaud, P. *J. Catal.* **2004**, *222*, 152−166.
(33) Menetrey, M.; Markovits, A.; Minot, C.; Vitto, A. D.; Pacchioni, G. *Surf. Sci.* **2004**, *549*, 294−304.
(34) Ealet, B.; Goniakowski, J.; Finocchi, F. *Phys. Rev. B* **2004**, *69* (1−9), 195413.
(35) Ashworth, T. V.; Pang, C. L.; Wincott, P. L.; Vaughan, D. J.; Thornton, G. *Appl. Surf. Sci.* **2003**, *210*, 2−5.
(36) Barth, C.; Henry, C. R. *Phys. Rev. Lett.* **2003**, *91* (1−4), 196102.
(37) Holt, S. A.; Jones, C. F.; Watson, G. S.; Crossley, A.; Johnston, C.; Sofield, C. J.; Myhra, S. *Thin Solid Films* **1997**, *292*, 96−102.
(38) Scarano, D.; Bertarione, S.; Spotto, G.; Zecchina, A. *Surf. Sci.* **2004**, *570*, 155−166.
(39) Kim, S.; Baik, S.; Kim, H. W.; Kim, C. Y. *Surf. Sci.* **1993**, *294*, L935−L938.
(40) Kim, S.; Baik, S. *Appl. Surf. Sci.* **1994**, *78*, 285−292.
(41) Costa, D.; Chizallet, C.; Ealet, B.; Goniakowski, J.; Finocchi, F. *J. Chem. Phys.* **2006**, in press.

(42) Knözinger, E.; Diwald, O.; Sterrer, M. *J. Mol. Catal. A: Chem.* **2000**, *162*, 83−95.
(43) Coluccia, S.; Tench, A. J.; Segall, R. L. *J. Chem. Soc., Faraday Trans. 1* **1979**, *75*, 1769−1779.
(44) Bailly, M. L.; Costentin, G.; Lauron-Pernot, H.; Krafft, J. M.; Che, M. *J. Phys. Chem. B* **2005**, *109*, 2404−2413.
(45) Sugawara, A.; Mae, K. *Surf. Sci.* **2004**, *558*, 211−217.
(46) Giese, D. R.; Lamelas, F. J.; Owen, H. A.; Plass, R.; Gajdardziska-Josifovska, M. *Surf. Sci.* **2000**, *457*, 326−336.
(47) Onishi, H.; Egawa, C.; Aruga, T. *Surf. Sci.* **1987**, *191*, 479−491.
(48) Wander, A.; Bush, I. J.; Harrison, N. M. *Phys. Rev. B* **2003**, *68* (1−4), 233405.
(49) Baudin, M.; Wojcik, M.; Hermansson, K. *Surf. Sci.* **1997**, *375*, 374−384.
(50) Perdew, J.; Wang, Y. *Phys. Rev. B* **1992**, *45*, 13244−13249.
(51) Kresse, G.; Hafner, J. *Phys. Rev. B* **1994**, *49*, 14251−14269.
(52) Kresse, G.; Furthmüller, J. *Comput. Mater. Sci.* **1996**, *6*, 15−50.
(53) Kresse, G.; Joubert, D. *Phys. Rev. B* **1999**, *59*, 1758−1775.
(54) Schintke, S.; Messerli, S.; Pivetta, M.; Patthey, F.; Libioulle, L.; Stengel, M.; De Vita, A.; Schneider, W. D. *Phys. Rev. Lett.* **2001**, *87* (1−4), 276801.
(55) D'Ercole, A.; Ferrari, A. M.; Pisani, C. *J. Chem. Phys.* **2001**, *115*, 509−518.
(56) Digne, M.; Sautet, P.; Raybaud, P.; Euzen, P.; Toulhoat, H. *J. Catal.* **2002**, *211*, 1−5.
(57) Frisch, M. J.; et al. *Gaussian 03*, revision C.02; Gaussian, Inc.: Wallingford CT, 2004.
(58) Sushko, P. V.; Gavartin, J. L.; Shluger, A. L. *J. Phys. Chem. B* **2002**, *106*, 2269−2276.
(59) Refson, K.; Wogelius, A.; Fraser, D. G.; Payne, M. C.; Lee, M. H.; Milman, V. *Phys. Rev. B* **1995**, *52*, 10823−10826.
(60) Foster, M.; D'Agostino, M.; Passno, D. *Surf. Sci.* **2005**, *590*, 31−41.
(61) De Leeuw, N. H.; Purton, J. A. *Phys. Rev. B* **2001**, *63* (1−9), 195417.
(62) Paganini, M. C.; Chiesa, M.; Giamello, E.; Coluccia, S.; Martra, G.; Murphy, D. M.; Pacchioni, G. *Surf. Sci.* **1999**, *421*, 246−262.
(63) Ricci, D.; Di Valentin, C.; Pacchioni, G.; Sushko, P. V.; Shluger, A. L.; Giamello, E. *J. Am. Chem. Soc.* **2003**, *125*, 738−747.
(64) Chiesa, M.; Martino, P.; Giamello, E.; Di Valentin, C.; Del Vitto, A.; Pacchioni, G. *J. Phys. Chem. B* **2004**, *108*, 11529−11534.
(65) Chiesa, M.; Paganini, M. C.; Spoto, G.; Giamello, E.; Di Valentin, C.; Del Vitto, A.; Pacchioni, G. *J. Phys. Chem. B* **2005**, *109*, 7314−7322.
(66) Gay, I. D.; Harrison, N. M. *Surf. Sci.* **2005**, *591*, 13−22.
(67) Shluger, A. L.; Sushko, P. V.; Kantorovich, L. N. *Phys. Rev. B* **1999**, *59*, 2417−2430.
(68) Sushko, P. V.; Shluger, A. L. *Surf. Sci.* **1999**, *421*, L157−L165.
(69) Branda, M. M.; Ferullo, R. M.; Belelli, P. G.; Castellani, N. J. *Surf. Sci.* **2003**, *527*, 89−99.
(70) Nicholas, J. B.; Kheir, A. A.; Xu, T.; Krawietz, T. R.; Haw, J. F. *J. Am. Chem. Soc.* **1998**, *120*, 10471−10481.
(71) Jensen, M. B.; Pettersson, L. G. M.; Swang, O.; Olsbye, U. *J. Phys. Chem. B* **2005**, *109*, 16774−16781.
(72) Diez, V. K.; Apesteguia, C. R.; Di Cosimo, J. I. *Catal. Today* **2000**, *63*, 53−62.
(73) Mekhemer, G. A. H.; Halawy, S. A.; Mohamed, M. A.; Zaki, M. I. *J. Phys. Chem. B* **2004**, *108*, 13379−13386.
(74) Zhang, W.; Wang, H.; Wei, W.; Sun, Y. *J. Mol. Catal. A: Chem.* **2005**, *231*, 83−88.
(75) Di Valentin, C.; Locati, C.; Pacchioni, G. *Chem. Phys. Chem.* **2004**, *5*, 642−651.
(76) Giordano, L.; Del Vitto, A.; Pacchioni, G.; Ferrari, A. M. *Surf. Sci.* **2003**, *540*, 63−75.
(77) Coluccia, S.; Baricco, M.; Marchese, L.; Martra, G.; Zecchina, A. *Spectrochim. Acta, Part A* **1993**, *49*, 1289−1298.
(78) Coluccia, S.; Marchese, L. *Catal. Today* **1998**, *41*, 229−238.
(79) Spotto, G.; Gribov, E. N.; Ricchiardi, G.; Damin, A.; Scarano, D.; Bordiga, S.; Lamberti, C.; Zecchina, A. *Prog. Surf. Sci.* **2004**, *76*, 71−146.
(80) Sauer, J.; Ugliengo, P.; Garrone, E.; Saunders, V. R. *Chem. Rev.* **1994**, *94*, 2095−2160.
(81) Pacchioni, G.; Minerva, T. *Surf. Sci.* **1992**, *275*, 450−458.
(82) Neyman, K.; Rösch, N. *Surf. Sci.* **1993**, *297*, 223−234.
(83) Soave, R.; Pacchioni, G. *Chem. Phys. Lett.* **2000**, *320*, 345−351.
(84) Xu, Y.; Li, J.; Zhang, Y.; Chen, W. *Surf. Sci.* **2003**, *525*, 13−23.
(85) Branda, M. M.; Belelli, P. G.; Ferullo, R. M.; Castellani, N. J. *Catal. Today* **2003**, *85*, 153−165.
(86) Cai, S.; Neyman, K. M.; Knözinger, H.; Rösch, N. *Surf. Sci.* **2001**, *479*, 169−182.
(87) Xu, C.; Goodman, D. W. *Chem. Phys. Lett.* **1997**, *265*, 341−346.
(88) Johnson, M. A.; Stefanovich, E. V.; Truong, T. N.; Günster, J.; Goodman, D. W. *J. Phys. Chem. B* **1999**, *103*, 3391−3398.
(89) Joubert, J.; Fleurat-Lessard, P.; Delbecq, F.; Sautet, P. *J. Phys. Chem. B* **2006**, *110*, 7392−7395.